Mutation Effect Investigation on Cytochrome C_{552} Protein Instability and Electron Transfer Improvement in the *Acidithiobacillus Ferrooxidans* Bacteria Respiratory Chain

Mahnaz Shojapour (biosh85@yahoo.com)
Payame Noor University Faculty of Basic Sciences
Faezeh Fatemi
Materials and Nuclear Fuel Research School, Nuclear Science and Technology Research Institute, Tehran, Iran
Marzieh Dehghan Shasaltaneh
University of Zanjan Faculty of Sciences
Somayeh Farahmand
Payame Noor University Faculty of Basic Sciences

Research Article

Keywords: Acidithiobacillus ferrooxidans, E121D mutation, MD simulation, RCY/Cytochrome c552 complex, Respiratory chain

Posted Date: June 4th, 2021

DOI: https://doi.org/10.21203/rs.3.rs-441104/v1

Abstract

Cytochrome c_{552} (Cyc_1) is a protein in the electron transport chain of the *Acidithiobacillus ferrooxidans (Af)* bacteria which obtain their energy from oxidation Fe^{2+} to Fe^{+3}. The electrons are directed through Cyc_2, RCY (rusticyanin), Cytochrome $c_{552,}$ and Cox aa_3 proteins to O_2. Cytochrome c_{552} protein consists of two chains, A and B. In the present study, a new mutation (E121D) in the A chain of cytochrome c_{552} protein was selected due to electron receiving from Histidine 143 of RCY. Then, the changes performed in the E121D mutant were evaluated by MD simulations analyzes. Cytochrome c_{552} and RCY proteins were docked by a Patchdock server. By E121D mutation, the connection between the two chains in Cytochrome c_{552} was enhanced by an additional hydrogen bond between Zn1388 and aspartate 121. Asp 121 in chain A gets farther from Zn 1388 in chain B. Therefore, the aspartate gets closer to Cu 1156 of the RCY leading to the higher stability of the RCY/Cytochrome c_{552} complex. Further, an acidic residue (Glu121) becomes a more acidic residue (Asp121) and improving the electron transfer to Cytochrome c_{552} protein. The results of RMSF analysis showed further ligand flexibility in mutation. This leads to fluctuation of the active site and increases redox potential at the mutation point and the speed of electron transfer. This study also predicts that in all respiratory chain proteins, electrons probably enter the first active site via glutamate and exit through the second active site of each respiratory chain protein and through histidine.

Introduction

Cytochrome c_{552} protein is an essential protein in the electron transport chain on the *Af* bacterium membrane. This bacterium is considered one of the main bacteria involved in the metals bioleaching process. Bioleaching is the process of extracting metals from their minerals by using microorganisms. The electrons are transmitted through several protein carriers including the Cyc_2, RCY, Cytochrome c_{552}, and Cox aa_3. Cyc_2 is a protein that is available in the external membrane of *Af.* This protein was proposed as the first electron receptor on the respiratory chain between iron (Fe^{2+}) and oxygen [1]. The terminal electron receptor is a cytochrome oxidase (Cox aa_3) in the cytoplasmic membrane. Apart from many other anaerobic respiratory chains, the bioenergetics metabolism of this organism involves several proteins with the highest redox potential and is encoded by *rus* and *petI* operons for the downward and upward pathways, respectively. Redox potential is considered as a measure of the tendency of the chemical species (e.g. aqueous solutions) to either gains or loses electrons. A solution with a higher reduction potential (more positive) has more tendency to gain electrons and vice versa. The path of the respiratory chain (downward pathway) could be Cyc_2 → RCY → Cytochrome c_{552} → Cox aa_3 → O_2 [2]. Biochemical studies have shown that Fe^{2+} is oxidized by Cyc_2, which is present in the outer membrane. In addition, the electrons are directed to O_2 through RCY and Cytochrome c_{552} periplasmic proteins, and finally, Cox aa_3 in the internal membrane [3–5]. These enzymes with molecular oxygen reduction eventually led to the production of water molecules [6, 7]. Each of these enzymes has two active sites, one associated with the previous protein to receive electrons (first active site) and the other associated with the next protein to release electrons (second active site). The electron transfer reason in the

respiratory chain is the redox potential difference at chain components, and there is a high correlation between the amount of redox potential and electron reception. The standard redox potential (E_0) is considered as a numerical measure of convenience which can be reductions to the structure or make it easy to accept the electrons. If E_0 is more positive, it means more readiness for electron acceptance, and if E_0 is more negative, it means more readiness for releasing the electron. Therefore, electrons can be freely transferred from a set with a lower E_0 to a higher E_0. In the electron transport chain, each receiver has a larger E_0 than the electron donator. The electrons are transferred from Cu 1156 of RCY to the heme A in Cytochrome c_{552} via charged residue interactions RCY and Cytochrome c_{552}. His143 of RCY was organized to create a stable interaction with Glu121 of Cytochrome c_{552} at RCY/Cytochrome c_{552} complex [8, 9].

Cytochrome c_{552} protein consists of two chains, A and B. E121 of Cytochrome c_{552} interacts with H143 of RCY via zinc-binding at RCY/Cytochrome c_{552} complex. Based on studies conducted in the third and fourth structures of Cytochrome c_{552} protein by PyMOL software, there are three zinc ions associated with histidine in each chain. In Chain A, we have H 39 to Zn (1187), H 97 to Zn (1188), and H 152 to Zn (1189). In Chain B, we have H 239 to Zn (1388), H 297 to Zn (1390), and H 352 to Zn (1389). There are six zinc ions in Cytochrome c_{552}, but only Zn 1388, which binds to histidine 239 in the chain B, is involved in connecting to both Cytochrome c_{552} chains (Fig. 1).

In addition, Zinc (1388) is involved in binding glutamate 121 of chain A in Cytochrome c_{552} to histidine 143 of RCY. In fact, Zn 1388 is involved in both the connection of two-chain A, B in Cytochrome c_{552} and the formation of the RCY/Cytochrome c_{552} complex. In other words, histidine 143 in RCY may act as histidine 239 in the Cytochrome c_{552} crystal dimer [8] (Fig. 2A& B).

Jafarpour *et al.* (2020) studied the effect of the mutation on the RCY second active site [10]. In the present study, the effect of the novel mutation (E121D) on the same type of bacterium at the Cytochrome c_{552} first active site was investigated to speed up the bioleaching process by MD simulation methods.

Materials And Methods

Homology-Based Modeling of Wild Type and Mutant Structures

A. ferrooxidans ATCC 23270 (Id code: B7JAQ6) was selected as a model using the UniProt database [11]. The Cytochrome c_{552} protein crystallographic structure with a resolution of 2.13 and 98% identity was proposed as a template structure by the I-TASSER server (PDB ID: 1h1o). 3D structures were generated using modeler software (version 9.12). And, 100 pdb files were designed with different angles by using Modeler software. Finally, the first 25 pdb files sorted from low to high according to DOPE were selected.

Docking

Molecular docking is a computational procedure that aims to predict the favored orientation of a ligand to its macromolecular target (receptor) when these are bound to each other to form a stable complex [12]. The protein ability (enzyme) to interact with small molecules to form a supramolecular complex plays an important role in protein dynamics, enhancing or inhibiting its biological function [13].

Setting up parameters for docking

The wild and mutated protein Cytochrome c_{552} required Zn 1388 as a ligand involved in the protein structure and action. Thus, the assembly calculations were done with the AutoDock software version 4.2 based on the Lamarck genetic algorithm and experimental free energy function. The box center was set on the 121 glutamate residue, and the size of the box was adjusted for the free turning of the ligand [14-16]. Finally, the Cytochrome c_{552} and RCY proteins were docked by the Patchdock server to check the status of the two proteins relative to each other [17].

Mutations

Initially, we used MUpro and I-stable servers to predict the stability of mutated protein. According to both servers, this mutation reduced protein stability (Table 1). The Cytochrome c_{552} mutant model was generated using PyMOL software at position 121 from glutamate to aspartate in wild protein and the mutant structure was saved as a PDB structure [18]. Some servers such as ProSA-web, Q Mean, verify 3D, and RAMPAGE support structural wild and mutant [19].

Simulation System Setup

To explore the structural effect on Cytochrome c_{552} protein due to E121D point mutation, comparative MD simulation studies were performed in GROMACS 5.1.4 package on an Ubuntu Linux system and GROMOS96 43a1 force-field [20-23]. The modeled protein was solvated in a cubic box by the SPC216 water model [24]. Then the system was neutralized by adding, 4 Na^+ and 12 Cl^- ions to replace the first SPC water molecule in all directions [25]. After 5000 steps of energy minimization, MD simulation was run in NVT and NPT groups. The first phase of the NVT was run for a period of 100 ps and the second phase of the NPT was done for 100 ps under the position restraints condition for heavy atoms [26]. Final MD was run for 100 ns, and the atomic coordinates were saved every two ps to identify the structural change in the conformation of the Cytochrome c_{552} protein [19]. Then, the results of the generated files were visualized with VMD (Visual molecular dynamics) software [27,28] and analyzed using standard software presented by GROMACS 5.1.4 [28].

pathway Analysis

MD simulation results were evaluated by using trajectory files obtained, and the structural behavior of wild and mutant structures was compared. Then, the comparative analysis was performed for wild and mutant types. In the next method, root mean square deviation (RMSD), Radius of gyration (Rg), Root Mean Square Fluctuation (RMSF), Solvent Accessible Surface Area (SASA), and Database of secondary

structure assignments for all Protein (DSSP) were analyzed. Finally, hydrogen bonds (H Bonds) shaped by special residues of the protein to the solvent at the time of simulation were calculated [23].

Results

Checking the quality of the model produced

Employing four servers including ProSA-web, QMEAN, RAMPAGE, and Verify 3D, the best model was selected before and after mutation. The overall model quality was additionally examined using ProSA-web along with QMEAN servers. Then, the standardized score was calculated, which is a total model quality index. The results of PorSA-web and QMEAN Z-score indicated that the models have desirable qualities. In addition, 81.52% of amino acids having a score of 3D-1D> = 0.2 in verify 3D and RAMPAGE with 98.9% residues in the allowed region. The wild-type and E121D mutant were visualized using PyMOL as shown in Figure 2A-B.

The hydrogen bonding results analysis in Glu, Asp 121 in wild-type and mutant protein using PyMOL software

The results showed that glutamate has four hydrogen bonds in the side chain with the surrounding molecules in wild-type. However, there is an extra hydrogen bond that binds the aspartate to Zn1388 of chain B in E121D mutation (Fig.3A-B).

Analysis of the results of the distance between Zn 1388 of chain B and Cu1156 of RCY to glutamate 121 and aspartate 121 (after mutation) chain A using PyMOL software.

In E121D mutation, an increase occurred in the distance between Zn1388 of chain B and aspartate 121 of chain A compared to glutamate 121 (2.2 angstroms in E121 and 4.4 in D121). Also, a decrease occurred in the distance between aspartate 121 of chain A and Cu1156 of RCY at RCY/Cytochrome c_{552} complex (16.9 angstroms in E121 and 15.3 in D121) (Fig. 4A-B).

The results of MD simulation analysis and effects mutation on stability and protein secondary structure

MD simulation was performed to study the configuration, and stability in the wild-type protein and the changes of these parameters in the mutant protein, for both types of proteins. In addition, MD simulation is considered a useful method to support the experimental results in protein mutations through structural specifications at the atomic level [29]. RMSD, RMSF, SASA, H-bonds, Rg, and DSSP were analyzed throughout the simulation time (Table 2, 3).

To find out the effect of the mutation on conformational changes and the stability of the protein structure, the RMSD of Cα atoms was calculated for both the wild-type and mutant compared to the original structure [19]. The RMSD plot of the wild and mutant structures indicated the convergence pattern during 100 ns simulations (Fig. 5A). Convergence obtained for wild and mutant structures confirmed that the mutant protein has less sustainability than the wild-type.

The RMSF of each residue was measured to assign the mutation effect on the residues' dynamic behavior in wild and mutant proteins [19]. Overall, the mutant protein had more flexibility (RMSF) than the wild-type (+0.0002 increase) [30]. The RMSF plan is plotted for wild and mutant structures, as shown in Figure 5B.

Intermolecular hydrogen bonding is the electrostatic force between two polar bonds. In this bonding, hydrogen is bonded covalently to the highly electronegative atoms like nitrogen and oxygen. H bond was calculated for wild and mutant types. The average number of H bonds for the mutated structure was 125.78 ± 4.52 and -2 number decreased compared to wild protein (Table 2). The difference in the mutant H bonds confirmed the flexibility of the mutant structure (Fig. 5C).

Rg determines the compression of the protein. As the radius of gyration is higher, the protein tends to be more unstable, unfolding, and low compact [31]. The values of Rg for mutated variants were 1.62 ± 0.001 nm, with a slight change (+0.01 increase) in protein folding and its compactness (Table 2) (Fig. 5D).

SASA indicates the level of protein access to the solvent [32]. The change in SASA measured the accessibility of the protein to the solvent in the wild and mutant structure during simulations (Fig. 5E). The average of SASA for the mutated structure was 103.10 ± 0.59 nm^2 and +1.23 increased compared to wild protein (Table 2).

Figure 6 shows the alterations in the secondary structure of the protein during the simulations. The DSSP scheme has been used to calculate the secondary structure of wild-type and mutant protein. The analysis of wild and mutant structures shows the number of amino acids involved in different structures and the increase or decrease in the number of amino acids in the structures. The most changes are related to the turn structure with an increase of 2.27 amino acids, and the α helix structure with a decrease of 1.27 amino acids. The bar graph of the secondary structure for wild-type and E121D mutant systems is shown in Figure 6A. The amount of Structure, coil, Turn, and beta bridge in the mutant protein has increased but, beta-sheet, alpha-helix, have diminished. The highest value is shown in the secondary structure of the two systems for coil and alpha-helix. And the largest change is related to the turn structure (1.24% increase), which is shown in Table 3.

Results of φ and ψ angle analysis of amino acids in wild and mutant proteins by Ramachandran method

The results were reported as diagrams of changes in angles according to time, to investigate the state of the protein at the mutation point. According to the angles φ and ψ before and after mutation using the Ramachandran method, it was found that the amino acid studied did not change significantly in terms of angles φ and ψ (Fig. 7, Table 4).

The Wild and mutant proteins Ramachandran scheme produced by PROCHECK

To compare the Ramachandran results of simulated wild and mutant protein (E121D), the pdb files were uploaded and the results are shown in Figure 8 and Table 5. Before the mutation, 95.5% of the amino

acids are present in most favored regions, which after the mutation, its amount has decreased to 84%. There were no amino acids in the allowed and disallowed regions before the mutation, but after the E121D mutation, two of the amino acids (alanine 9, histidine 54) were in the allowed regions.

Discussion

Following previous studies, E121D mutation at the first active site and the electron entry point from the RCY to Cytochrome c_{552} were conducted on *Af* bacterium. Molecular dynamics simulation studies on wild-type and mutant identified the influence of mutations at the active site. The trajectory analysis was used to calculate protein changes and showed the changes in protein structure associated with increased flexibility at the mutation point (+ 0.0017 increase).

DSSP is an algorithm that deals with information on the secondary structure of proteins [33]. DSSP analysis aims to measure the content of the secondary structure of a protein as a function of time. The analysis of the wild and mutated structures shows the number of amino acids involved in different structures, as well as increasing or decreasing the number of amino acids in the structure. In the DSSP scheme, with the conversion of glutamate to aspartate, structure, coil, β Bridge, and Turn increased by 0.62%, 0.08%, 0.09% and 1.24%, respectively, and β Sheet, α helix, 5-helix, and 3-helix decreased by 0.006%, 0.69%, 0.48%, and 0.11%, respectively. A decrease of 0.69% in the alpha-helix in the DSSP plan is related to the fact that aspartate tends to disrupt a helix because their side chains contain hydrogen-bond donors or acceptors in proximity to the main chain, where they compete for main-chain NH and CO groups [34]. The number of amino acids which participate in protein structure eventually increased by 0.62% (Table 3).

As mentioned, the *Af* bacterium is considered as one of the main bacteria involved in the metal bioleaching process, and bioleaching is the extraction of metals from their minerals through using these bacteria [11]. RCY and Cytochrome c_{552} are considered as consecutive proteins in the electron transport chain *Af* bacterium. In this way, the electron is transmitted from RCY to Cytochrome c_{552} [9].

Patra *et al*. indicated that His143 of RCY has a stable interaction with Glu121 of periplasmic Cytochrome c_{552}. In addition, glutamate 121 is associated with iron and causes electron transfer to heme A [9].

Malarte *et al.* evaluated glutamate 121, which played a key role in the formation of the RCY/Cytochrome c_{552} complex. They found that the complex was destroyed by the E121A mutation and the conversion of an electrically charged glutamate to a hydrophobic alanine [35]. The formation of the complex significantly modified the pK value of the exposed histidine ligand to the Cu ion and regulated the midpoint potential of the redox in the site of Cu [36]. Abergel *et al*. reported the role of the divalent Zn cation, which prevents RCY/Cytochrome c_{552} interaction by making E121 unavailable [8]. The results of MD analysis demonstrate the effect of E121D mutation on the unfolding of the cytochrome c_{552} protein and the increased distance between Zn 1388 and aspartate 121 (4.4 angstroms instead of 2.2 angstroms for glutamate). Moreover, there is a decrease in the distance between Cu 1156 in RCY and the

Cytochrome c_{552} aspartate 121, which creates a more stable RCY/Cytochrome c_{552} complex (15.3 angstroms instead of 16.9 angstroms for glutamate) (Fig. 4A-B). The kd value of glutamate for zinc ions and copper ions is $10^{-5.5}$ and 10^{-8} at pH 4.5, respectively (the lower kd value leads to the higher binding affinity of the ligand to its target) [8]. The glutamate interacts with zinc inhibiting the interaction with Rusticyanin. Further, with E121D mutation, the role of zinc inhibiting on the Asp 121 Cytochrome c_{552} decreases and one could expect shorter distances with the Rustycianin copper. Therefore, its tendency to copper 1156 of RCY increases, and the RCY/Cytochrome c_{552} complex becomes more stable after the mutation.

In this study, we proposed the novel E121D mutation in which glutamate has four hydrogen bonds in the side chain with the surrounding molecules. However, in aspartate, there is an extra hydrogen bond that binds this amino acid to Zn1388 in the B chain and creates a stronger bond between the two chains (Fig. 3A-B).

Abergel et al. reported that histidine is deprotonated due to the 3.2 Å distance between Nε H143 and Oγ E12, and their formation of hydrogen bonds between. The RCY redox potential decreases and, consequently, the transfer of electrons from the RCY to Cytochrome c_{552} is more efficient [8]. This mutation converts an acidic residue into a more acidic residue Therefore, His143 becomes more deprotonated, reduces the redox potential at the RCY midpoint, and improves electron transfer to Cytochrome c_{552} protein at RCY/Cytochrome c_{552} complex.

Also, the results of RMSF analysis show more flexibility in the mutation point compared to the wild type. The E121D mutation reduces stability at the active site. Finally, instability of the active site leads to increased ligand flexibility (ΔS) and ΔG decrease and increase in the value of E_0 which is proved by two formulas Gibbs free energy ($\Delta G = \Delta H - T\Delta S$) and Nernst ($E_0 = -\Delta G/nF$) [37]. Finally, by the increase in redox potential, electron transfer from RCY to Cytochrome c_{552} at RCY/Cytochrome c_{552} complex is accelerated. In this groundbreaking study, we found that in all respiratory chain proteins, electrons probably enter through the glutamate in the first active site and exit through histidine at the second active site of each respiratory chain protein. Therefore, by converting glutamate to aspartate at the electron entry point and converting histidine to arginine at the electron exit point, and destabilizing the active site of each protein in the respiratory chain, the electron transfer rate in the chain, followed by the bioleaching process, can be improved.

Conclusion

Based on the results, the mutated protein (E121D) is unfolded more than wild protein. The analysis of the hydrogen bond indicates that the mutant protein is more flexible. However, in aspartate, there is an extra hydrogen bond that binds this amino acid to Zn1388 in the B chain and creates a stronger bond between the two chains. By converting glutamate 121 to aspartate, a decrease occurs in the role of zinc inhibiting on the Asp 121 Cytochrome c_{552}. Therefore, the aspartate gets closer to Cu 1156 of the RCY and results

in higher stability of the RCY/Cytochrome c_{552} complex. On the other hand, an acidic residue (Glu121) becomes a more acidic residue (Asp121), and His143 is more deprotonated inducing a reduction of the redox potential at the rusticyanin midpoint improving the electron transfer to Cytochrome c_{552} protein. Also, by the increase in flexibility and decreasing ΔG in the active site, the redox potential at the mutation point increases, and the electron transfer to Cytochrome c_{552} improves. For future studies, we propose extensive research on electron transfer improvement by selecting the best mutations obtained by bioinformatics methods at all active sites (electron entry and exit points) in all respiratory chain proteins. In this way, The amino acids in the first active site of the proteins, namely glutamate, are converted to aspartate with more acidic properties. And the amino acid histidine converted to the more alkaline amino acid arginine in the second active site position. As a result, the active site becomes more unstable and the speed of electron transfer in the chain increases. Finally, biotechnological methods can clone bacteria that have the above mutations to improve the bioleaching process.

Declarations

Funding

No funding was received for conducting this study.

Acknowledgments

We also thank Ms. Saba Miri for her valuable technical advice.

Author contribution

The protocol designed, conceptualized by F.F., Manuscript preparation, and analysis, and supervision is done by M.Sh. General consultation of the project and editing of the manuscript was done by M.D.Sh. Part of the text editing was done by S.F. The manuscript was reviewed and approved by all authors.

Data Availability Statement

The analyses during the current study are available from the corresponding author on reasonable request.

Conflict of Interest

The authors declare that they have no conflicts of interest to this work.

References

1. Fatemi F, Miri S, Jahani, S (2017) Effect of metal sulfide pulp density on gene expression of electron transporters in *Acidithiobacillus* sp. FJ2. *Arch Microbiol, 199*(4): 521-530. DOI: 10.1007/s00203-016-1318-1

2. Rawlings D. E (2005) Characteristics and adaptability of iron-and sulfur-oxidizing microorganisms used for the recovery of metals from minerals and their concentrates. *MICROB CELL FACT*. 4, 13. https://doi.org/10.1186/1475-2859-4-13
3. Ingledew W. J (1982) Thiobacillus ferrooxidans the bioenergetics of an acidophilic chemolithotroph. *BBA-BIOENERGETICS*. 683, 89-117. https://doi.org/10.1016/0304-4173(82)90007-6
4. Holmes D. S, Bonnefoy V (2007) Genetic and bioinformatic insights into iron and sulfur oxidation mechanisms of bioleaching organisms. Biomining, Springe. 281-307. https://doi.org/10.1007/978-3-540-34911-2_14
5. Yarzabal A, Appia-Ayme C, Ratouchniak J, & Bonnefoy V (2004) Regulation of the expression of the Acidithiobacillus ferrooxidans rus operon encoding two cytochromes c, a cytochrome oxidase and rusticyanin. *Microbiology +*, 150(7), 2113-2123. DOI:10.1099/mic.0.26966-0
6. Bruscella P, Appia-Ayme C, Levican G, Ratouchniak J, Jedlicki E, Holmes D. S, et al (2007) Differential expression of two bc1 complexes in the strict acidophilic chemolithoautotrophic bacterium Acidithiobacillus ferrooxidans suggests a model for their respective roles in iron or sulfur oxidation. *Microbiology +*, 153(1), 102-110. DOI 10.1099/mic.0.2006/000067-0
7. Lyons J. A, Aragão D, Slattery O, Pisliakov A. V, Soulimane, T, Caffrey, M (2012) Structural insights into electron transfer in caa 3-type cytochrome oxidase. *Nature*, 487(7408), 514. https://doi.org/10.1038/nature11182
8. Abergel C, Nitschke W, Malarte G, Bruschi M, Claverie, J.-M, Giudici-Orticoni, M.-T (2003) The structure of Acidithiobacillus ferrooxidans c4-cytochrome: a model for complex-induced electron transfer tuning. *Structure*, 11(5), 547-555. DOI:10.1016/S0969-2126(03)00072-8
9. Patra M. C, Pradhan S K, Rath S N, Maharana J (2013) Structural Analysis of Respirasomes in Electron Transfer Pathway of Acidithiobacillus ferrooxidans: A Computer-Aided Molecular Designing Study. *ISRN Biophysics*, 2013. http://dx.doi.org/10.1155/2013/295718
10. Jafarpour R, Fatemi F, Eidi A, & Mehrnejad F (2020) Effect of the Met148Leu Mutation on the Structure and Dynamics of the Rusticyanin Protein from Acidithiobacillus sp. FJ2. Biomol Struct Dyn (just-accepted), 1-19. https://doi.org/10.1080/07391102.2020.1775119
11. Jahani S, Fatemi F, Firoz-e-zare M, Zolfaghari, M (2015) Isolation and characterization of Acidithiobacillus ferrooxidans strain FJS from Ramsar, Iran. *Electronic J Biol*, 11(4), 138-146.
12. Lengauer T, & Rarey, M (1996) Computational methods for biomolecular docking. Curr. Opin. Struct. Biol, 6(3), 402-406. https://doi.org/10.1016/S0959-440X(96)80061-3
13. Hernández-Santoyo A, Tenorio-Barajas A. Y, Altuzar V, Vivanco-Cid H, Mendoza-Barrera C (2013) Protein-protein and protein-ligand docking. Protein engineering-technology and application. http://dx.doi.org/10.5772/56376
14. Abdel-Hamid M. K, McCluskey A (2014) In Silico docking, molecular dynamics and binding energy insights into the bolinaquinone-clathrin terminal domain binding site. *Molecules*, 19(5), 6609-6622. https://doi.org/10.3390/molecules19056609

15. Dehghan-Shasaltaneh M, Lanjanian H, Riazi G. H, & Masoudi-Nejad, A (2018) The importance of α-CT and Salt bridges in the Formation of Insulin and its Receptor Complex by Computational Simulation. Iran J Pharm Res: IJPR, 17(1), 63. available online at http://www.ijpr.ir
16. Ling B, Zhang R, Wang Z, Liu Y, & Liu C (2010) Study on the interactions of SMAC mimetics with XIAP-BIR3 domain by docking and molecular dynamics simulations. J THEOR COMPUT CHEM, 9(04), 797-812. DOI: 10.1142/S0219633610005980
17. DeLano W. L (2002) Pymol: An open-source molecular graphics tool. *CCP4 Newsletter on protein crystallography*, 40(1), 82-92.
18. Ghasemi F, Zomorodipour A, Karkhane A. A, Khorramizadeh M. R (2016) In silico designing of hyper-glycosylated analogs for the human coagulation factor IX. Journal of J Mol *Graph Model*, 68, 39-47. DOI: 10.1016/j.jmgm.2016.05.011
19. van Gunsteren W. F, Billeter S. R, Eising A. A, Hünenberger P. H, Krüger P, Mark A. E, et al. (1996) *Biomolecular simulation*: the {GROMOS96} manual and user guide.
20. Imani S, Cheng J, Shasaltaneh M. D, Wei C, Yang L, Fu S, et al. (2017) Genetic identification and molecular modeling characterization reveal a novel PROM1 mutation in Stargardt4-like Macular Dystrophy. *ONCOTARGET*. doi: 10.18632/oncotarget.22343. eCollection 2018 Jan 2
21. Castelle C, Guiral M, Malarte G, Ledgham F, Leroy G, Brugna M, et al. (2008) A new iron-oxidizing/O2-reducing supercomplex spanning both inner and outer membranes, isolated from the extreme acidophile Acidithiobacillus ferrooxidans. *J BIOL CHEM*, 283(38), 25803-25811. DOI:10.1074/jbc.M802496200
22. Srikumar P, & Rohini K (2013) Exploring the structural insights on human laforin mutation K87A in Lafora disease—a molecular dynamics study. *Appl Biochem Biotechnol*, 171(4), 874-882.
23. Berendsen H, Grigera J, & Straatsma T (1987) The missing term in effective pair potentials. Journal of Physical Chemistry, 91(24), 6269-6271.
24. Linder T, Wang S, Zangerl-Plessl E.-M, Nichols C. G, & Stary-Weinzinger A (2015) Molecular dynamics simulations of KirBac1. 1 mutants reveal global gating changes of Kir channels. Journal of chemical information and modeling, 55(4), 814-822. DOI: 10.1021/acs.jcim.5b00010
25. Berendsen H. J, Postma J. v, van Gunsteren W. F, DiNola A, & Haak J (1984) Molecular dynamics with coupling to an external bath. *J PHYS CHEM-US*, 81(8), 3684-3690. DOI: 10.1007/s12010-013-0393-x
26. Humphrey W, Dalke A, Schulten K (1996) VMD: visual molecular dynamics. J. Mol. Graph, 14(1), 33-38. https://doi.org/10.1016/0263-7855(96)00018-5
27. Hess B, Kutzner C, Van Der Spoel D, & Lindahl E (2008) GROMACS 4: algorithms for highly efficient, load-balanced, and scalable molecular simulation. *J CHEM THEORY COMPUT*, 4(3), 435-447. DOI: 10.1021/ct700301q
28. Dodson G. G, Lane D. P, Verma C. S (2008) Molecular simulations of protein dynamics: new windows on mechanisms in biology. *EMBO reports*, 9(2), 144-150. DOI: 10.1021/ct700301q
29. Zhao Y, Zeng C, & Massiah M. A (2015) Molecular dynamics simulation reveals insights into the mechanism of unfolding by the A130T/V mutations within the MID1 zinc-binding Bbox1 domain.

PLoS One, 10(4).

30. Lobanov M. Y, Bogatyreva N. Galzitskaya O (2008) Radius of gyration as an indicator of protein structure compactness. *Mol Biol+*, 42(4), 623-628. DOI: 10.1134/S0026893308040195
31. Satpati S, Manohar K, Acharya N, Dixit A (2017) Comparative molecular dynamics studies of heterozygous open reading frames of DNA polymerase eta (η) in pathogenic yeast Candida albicans. *SCI REP-UK*, 7, 41087. https://doi.org/10.1038/srep41087
32. Kabsch W, Sander C (1983) Dictionary of protein secondary structure: pattern recognition of hydrogen-bonded and geometrical features. *BIOPOLYMERS*, 22(12), 2577-2637. https://doi.org/10.1002/bip.360221211
33. Berg J. M, Tymoczko J. L, & Stryer L (2013) Das Immunsystem. *In Stryer Biochemie*, pp. 993-1024.
34. Malarte G, Leroy G, Lojou E, Abergel C, Bruschi M, Giudici-Orticoni, M. T. (2005). Insight into molecular stability and physiological properties of the diheme cytochrome CYC41 from the acidophilic bacterium Acidithiobacillus ferrooxidans. *Biochemistry*, 44(17), 6471-6481. DOI: 10.1021/bi048425b
35. Marie-Thérese Giudici-Orticoni F, Guerlesquin M. B, & Nitschke W (1999) Interaction-induced Redox Switch in the Electron Transfer Complex Rusticyanin-Cytochrome c4. J BIOL CHEM DOI: 10.1074/jbc.274.43.30365

Tables

Table. 1 Protein stability upon mutation at 27°C and pH = 2, using two servers MUpro and I-Mutant 2.0.

MUpro		I-Mutant 2.0	
Stability	DDG (Kcal/mol)	Stability	DDG (Kcal/mol)
Decrease	-1.25	Decrease	-0.18

DDG<0: Decrease of Stability, DDG>0: Increase of Stability.

Table. 2 The average of RMSD, RMSF, SASA, H-Bonds, and Rg values of Wild and E121D Mutant.

Parameters	Wild	E121D Mutant
RMSD	0.0241±0.001	0.0243±0.001
RMSF	0.0202±0.002	0.0204±0.002
Rg	1.61±0.001	1.62±0.001
SASA	101.87±0.52	103.10±0.59
NH bonds	127.54±4.03	125.78±4.52

The values of RMSD, RMSF and Rg are given in nm, values of SASA given in nm^2, and values of NH bonds given in numbers.

Table. 3 the secondary structure average for Wild and E121D Mutant during the 100 ns MD simulation.

Secondary Structure	Wild type	Wild type (%)	E121D Mutant	E121D Mutant (%)	Difference amount
Structure	109.52 ± 3.37	59.52	110.66 ± 2.71	60.14	1.14 (0.62%) ↑
Coil	50.52 ± 1.14	27.45	50.68 ± 1.02	27.54	0.16(0.08%) ↑
B-Sheet	0.10 ± 0.69	0.054	0.09 ± 0.64	0.048	0.01(0.006%) ↓
B-Bridge	4.33 ± 1.045	2.35	4.5 ± 1.26	2.44	0.17(0.09%) ↑
Turn	22.59 ± 2.66	12.27	24.86 ± 2.22	13.51	2.27(1.24%) ↑
A-Helix	82.49 ± 2.41	44.83	81.22 ± 1.21	44.14	1.27(0.69%) ↓
5-Helix	5.85 ± 2.06	3.18	4.98 ± 1.53	2.70	0.87(0.48%) ↓
3-Helix	0.79 ± 1.35	0.43	0.59 ± 1.21	0.32	0.20(0.11%) ↓

Table. 4 Average, minimum and maximum values of dihedral angles φ and ψ during simulation in Wild and E121D protein.

Wild				E121D			
GLU121	Average	min	max	ASP121	Average	min	max
	φ				φ		
	-55.31±7.80	-80.41	-25.52		-55.69±8.35	-84.14	-26.18
	ψ				ψ		
	-50.42±9.84	-84.71	-23.38		-59.34±11.22	-89.07	-26.23

Table. 5 Comparison of statistical parameters of Ramachandran plot for Wild and E121D protein.

Status of the residues in the Ramachandran plot	amino acids Number (Wild)	amino acids Number E121D	amino acids Percentage Wild	amino acids Percentage E121D
Residues in most favored regions [A,B,L]	149	131	95.5	84
Residues in additional allowed regions [a,b,l,p]	7	23	4.5	14.7
Residues in generously allowed regions [~a,~b,~l,~p]	0	2	0	1.3
Residues in disallowed regions	0	0	0	0
Number of non-glycine and non-proline residues	156	156	100	100
Number of end-residues (excl. Gly and Pro)	2	2		
Number of glycine residues (shown as triangles)	16	16		
Number of proline residues	10	10		
Total number of residues	184	184		

Figures

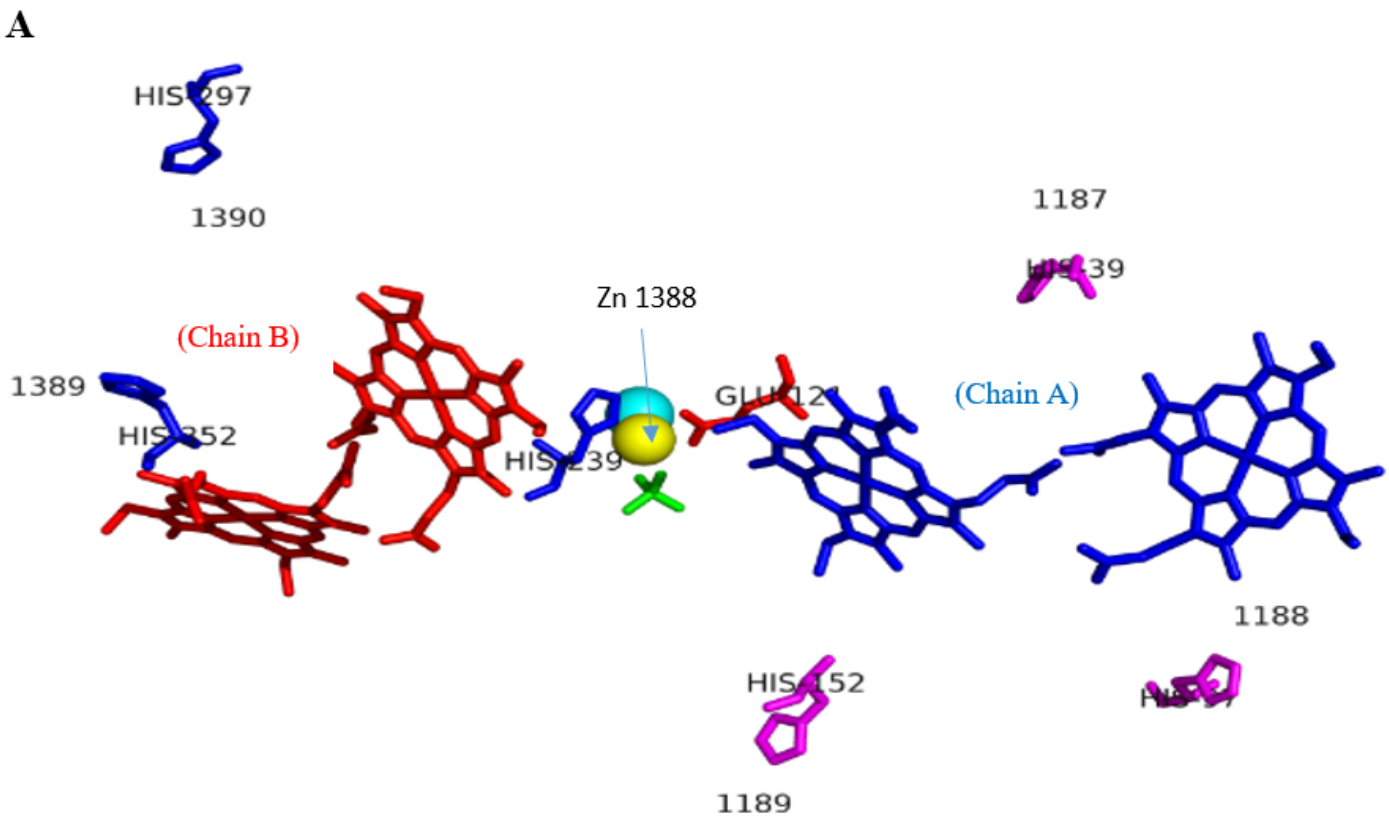

Figure 1

There are six zinc ions in Cytochrome c552. (A) Three zinc ions are associated with histidine in each chain. In Chain A, H 39 to Zn (1187), H 97 to Zn (1188), and H 152 to Zn (1189) and shown in Purple. In Chain B, H 239 to Zn (1388), H 297 to Zn (1390), and H 352 to Zn (1389) and shown in dark blue. Zn 1388, which binds to histidine 239 in chain B, is involved in connecting to both Cytochrome c552 chains and shown in yellow and H2O 2068 in blue, and SO4 1387 in green.

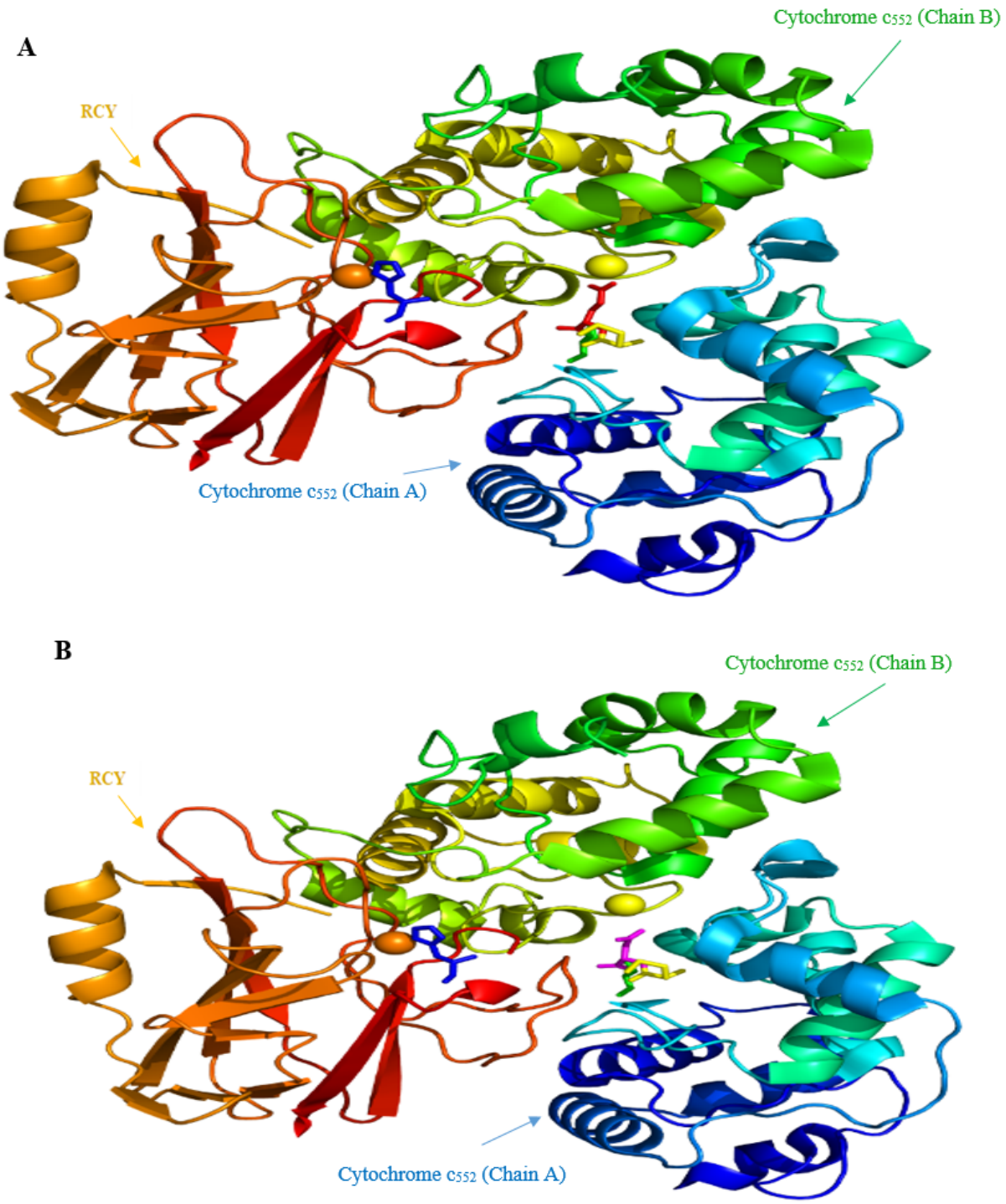

Figure 2

Structure of the RCY/Cytochrome c552 complex (chain A of Cytochrome c552: Light and dark blue, chain B of Cytochrome c552: green and yellow: RCY: red and brown). (A) Wild: Glu121 of chain A, red and His 143 of RCY, dark blue, Zn 1388 of chain B, yellow and Cu 1156 of RCY, orange. (B) E121D mutant: Asp121 of chain A, pink and His 143 of RCY, dark blue, Zn 1388 of chain B, yellow and Cu 1156 of RCY, orange.

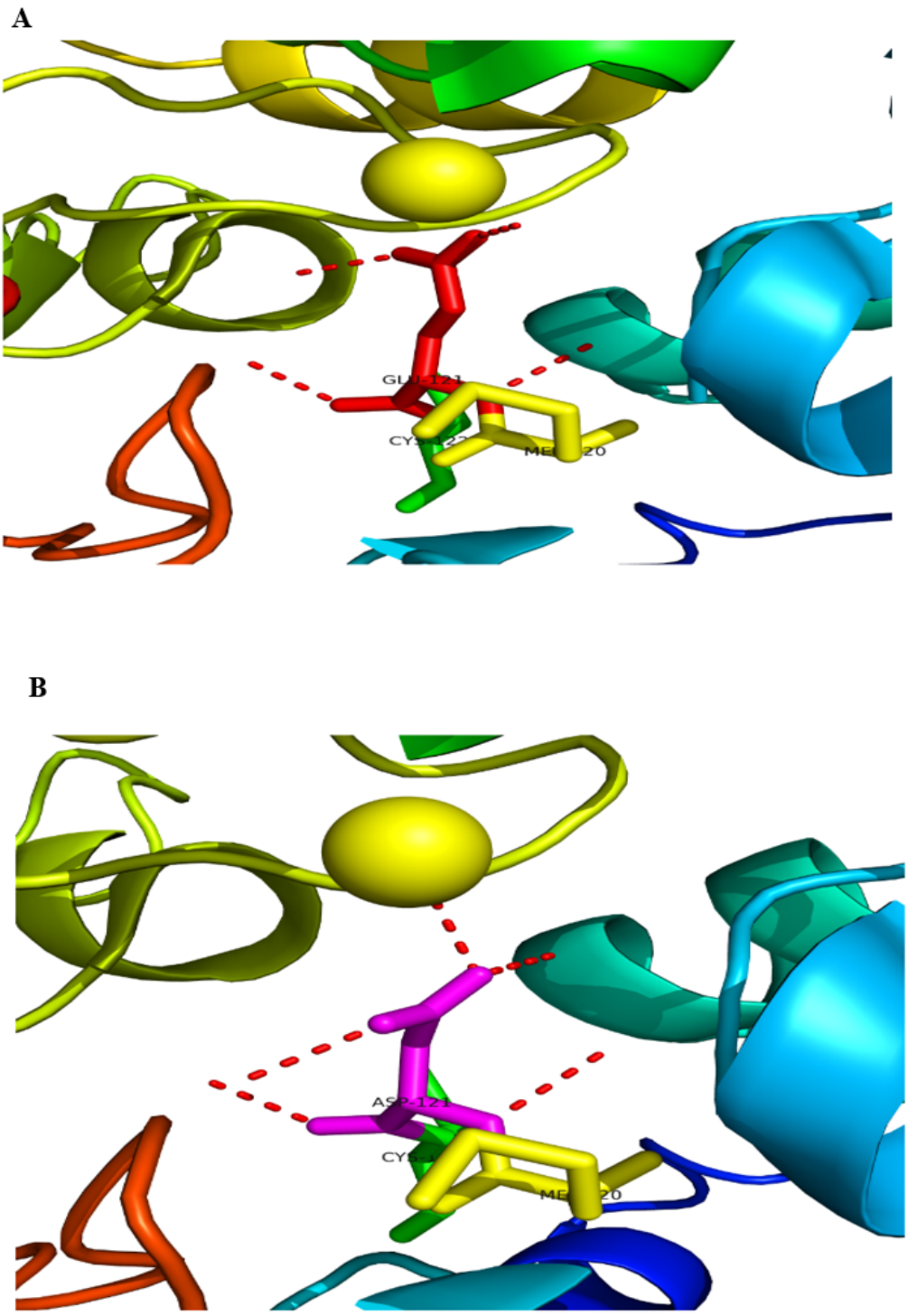

Figure 3

Effect of hydrogen bonds on the stability of the RCY/Cytochrome c552 complex after mutation. (A) The hydrogen bond of Glu 121 (red) in the wild and (B) The hydrogen bond of Asp 121 (pink), in E121D mutant is marked with red dotted lines which were prepared by PyMOL software.

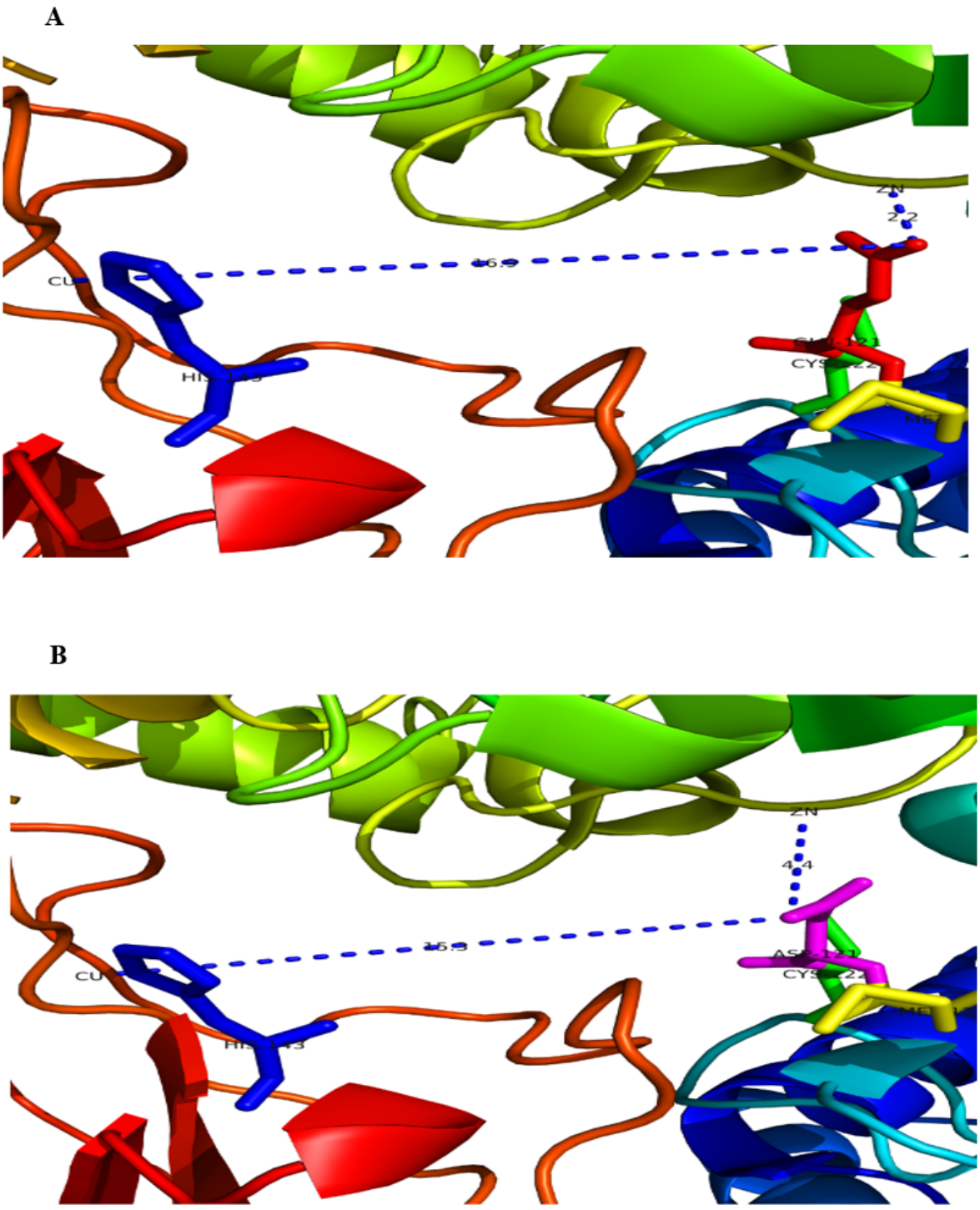

Figure 4

The effect of mutation on reducing the distance and stability of RCY/Cytochrome c552 complex (A) The distances of the glutamate 121 in chain A to Zn 1388 in chain B and the distances of the glutamate 121 in chain A to Cu1156 of RCY. (B) The distances of the aspartate 121 in chain A to Zn 1388 in chain B and the distances of the aspartate 121 in chain A to Cu1156 of RCY are marked with blue dotted lines which were prepared by PyMOL software.

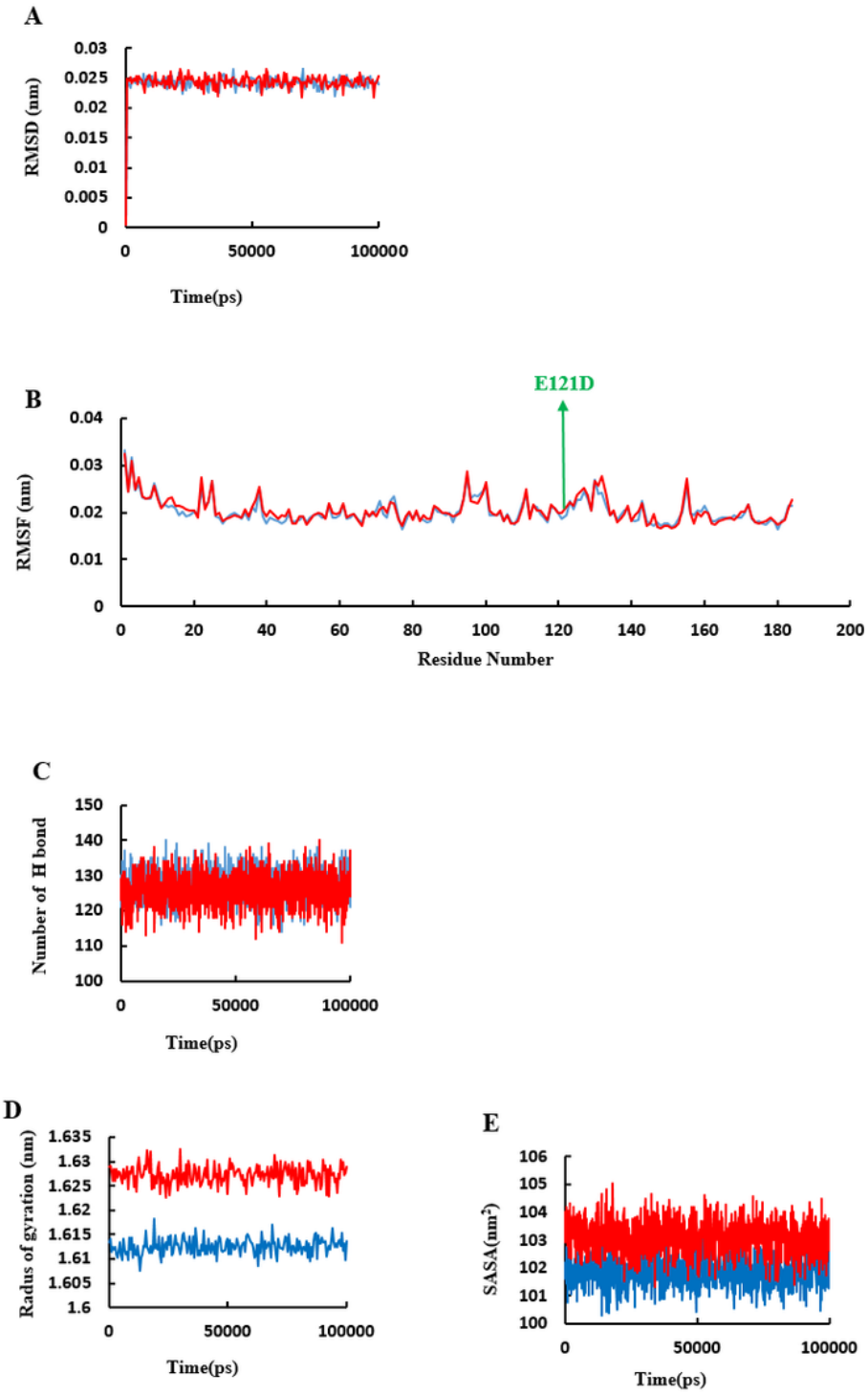

Figure 5

Functional effects of the E121D mutation on Cytochrome c552 protein. (A) RMSD plots of backbone atoms of the wild-type and E121D complex systems for 100 ns of simulation, where time step is plotted on X-axis and RMSD (nm) is plotted on Y-axis. (B) Cα-RMSF plots of the wild-type and E121D complex system for 100 ns of simulation, where residue number is plotted on the X-axis while RMSF (nm) is plotted on the Y-axis. (C)The number of H bonds is plotted where there is a time step on X-axis while NH

bonds are plotted on Y-axis. (D) The Radius of gyration (Rg) is plotted where there is a time step on X-axis while Rg is plotted on Y-axis. (E) SASA is plotted where there is a time step on X-axis while SASA (nm) is plotted on Y-axis. The mutation diagrams (E121D) have been shown in red and the wild-type in blue.

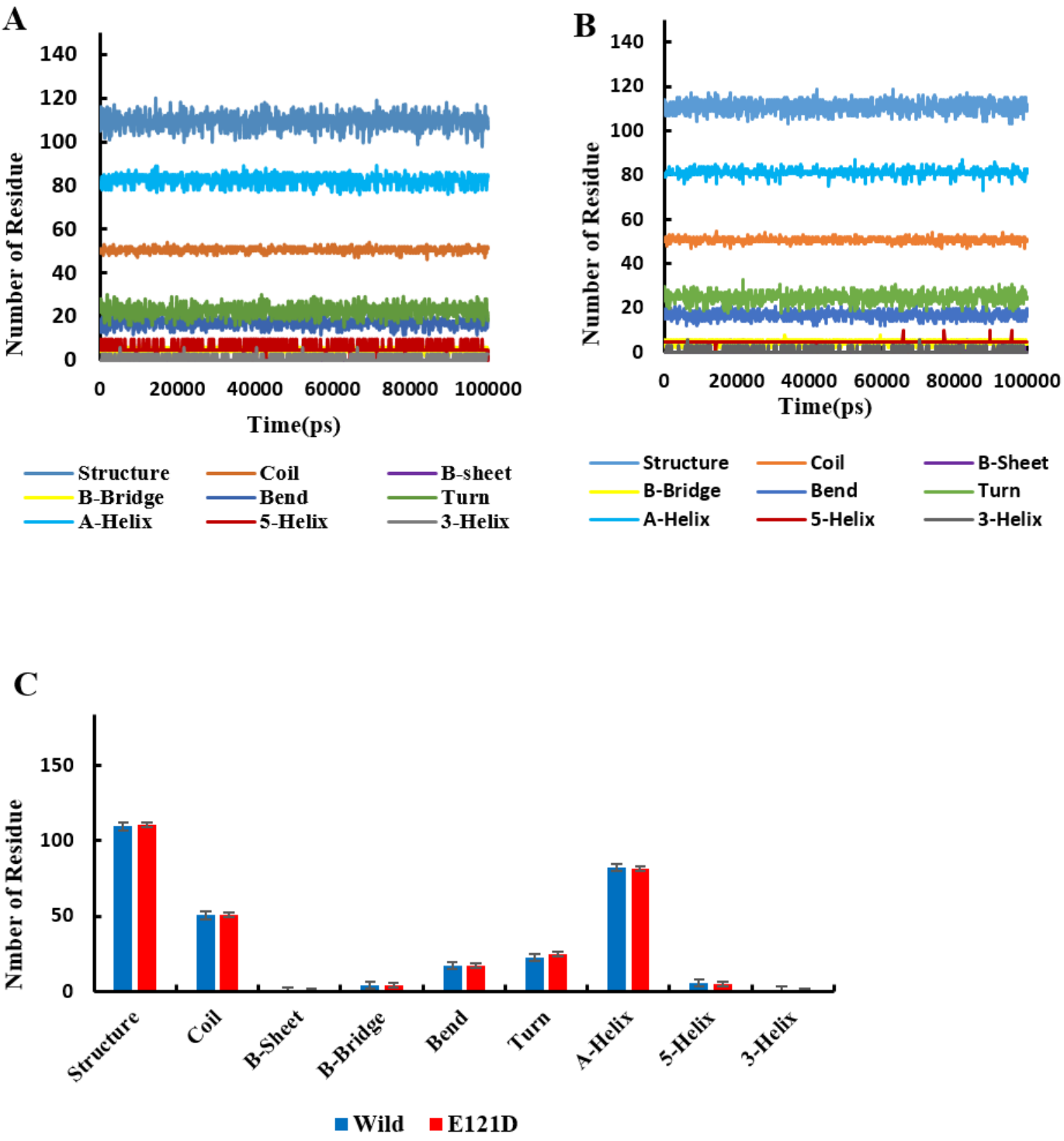

Figure 6

Secondary structure analysis of wild-type in comparison with the mutant form (E121D). (A & B) The DSSP plots (100 ns) of wild-type and E121D mutant systems at 300 K. (C) The bar graph of the residue

number of secondary structure for wild-type and the mutant.

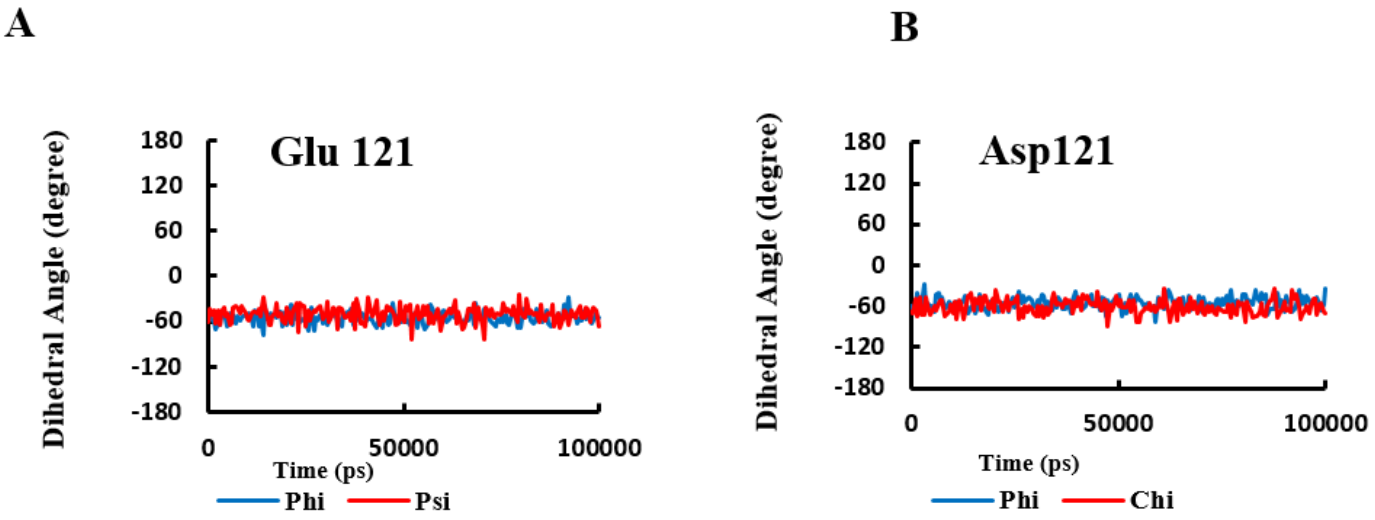

Figure 7

Dihedral Angles φ and ψ of Amino Acid Glu121, Asp121 in Wild and Mutant E121D Protein.

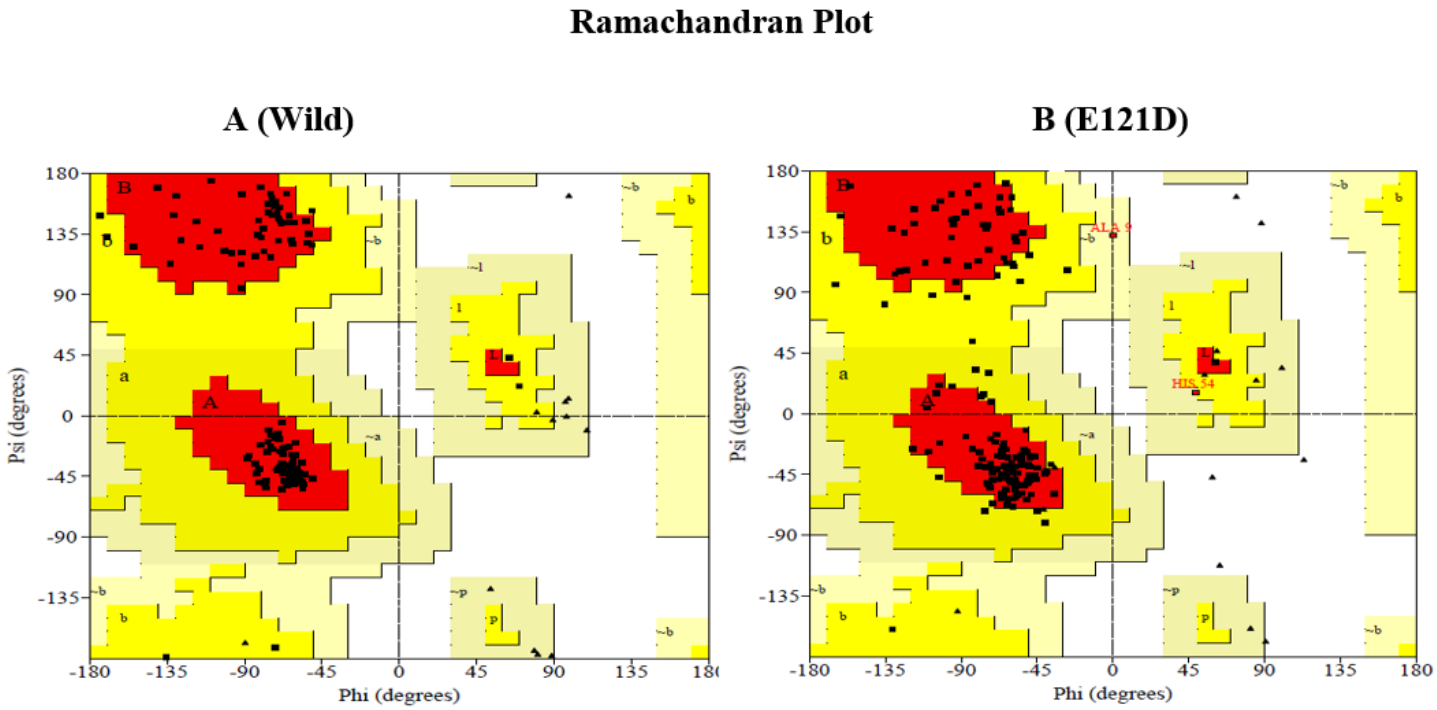

Figure 8

Ramachandran scheme to investigate the status of amino acids in Wild and Mutant E121D proteins generated by PROCHECK. Red indicates the most favored regions, yellow indicates allowed regions, beige indicates tolerated regions and white indicates unfavorable regions.

Supplementary Files

This is a list of supplementary files associated with this preprint. Click to download.

- Graphicalabstract.docx